ELSEVIER

Diamond and Related Materials 10 (2001) 370–375

DIAMOND AND RELATED MATERIALS

www.elsevier.com/locate/diamond

Diamond deposition in a DC-arc Jet CVD system: investigations of the effects of nitrogen addition

J.A. Smith, K.N. Rosser, H. Yagi[1], M.I. Wallace[2], P.W. May, M.N.R. Ashfold*

School of Chemistry, University of Bristol, Bristol BS8 1TS, UK

Abstract

Studies of the chemical vapour deposition of diamond films at growth rates $> 100\ \mu m\ h^{-1}$ with a 10-kW DC-arc jet system are described. Additions of small amounts of N_2 to the standard $CH_4/H_2/Ar$ feedstock gas results in strong CN(B → X) emission, and quenches $C_2(d \rightarrow a)$ and H_α emissions from the plasma. Species selective, spatially resolved optical emission measurements have enabled derivation of the longitudinal and lateral variation of emitting C_2, CN radicals and H ($n = 3$) atoms within the plasma jet. Scanning electron microscopy and laser Raman analyses indicate that N_2 additions also degrade both the growth rate and quality of the deposited diamond film; the latter technique also provides some evidence for nitrogen inclusion within the films. © 2001 Elsevier Science B.V. All rights reserved.

Keywords: Diamond growth; DC arc plasma jet; Chemical vapour deposition; Optical emission; Nitrogen additions

1. Introduction

DC-arc jet plasmas operating with hydrocarbon/H_2/Ar gas mixtures enable chemical vapour deposition (CVD) of high quality diamond films at growth rates unobtainable using the more traditional hot filament or microwave reactors [1]. The DC-arc jet, therefore, provides an excellent environment in which to study the mechanism of diamond CVD. Due to the low residence time, the chemical mechanism is much simplified in comparison with hot filament or microwave systems allowing modelling of the plasma plume, given accurate measurements of the boundary conditions [2,3]. The high temperatures and the large reactive radical flux complicate diagnostic measurements, but spatially resolved optical emission and laser-induced fluorescence (LIF) measurements have been reported for several species in DC-arc plasma jet reactors [4].

The present contribution describes studies of nitrogen addition to a twin-torch DC-arc plasma jet operating with a $CH_4/H_2/Ar$ gas mixture, both in terms of the characteristics of the films produced and its influence on the gas phase chemistry. Related studies of the effects of N_2 additions have been reported in the case of diamond CVD using hot filament [5,6], microwave [7–9] and oxy-acetylene torch [10] reactors. All show a peak in growth rate and film quality with the introduction of appropriate trace amounts of N_2; controlled addition of N_2 has also been shown to induce selective facet formation in these diamond CVD systems.

Films grown in the present study have been analysed by scanning electron microscopy (SEM) and laser Raman spectroscopy (LRS). The DC-arc plasma jet thus far has been monitored by spatially resolved optical emission spectroscopy (OES) only, with particular reference to emissions from electronically excited H atoms,

* Corresponding author. Tel.: +44-117-928-8312/3; fax: +44-117-925-0612.

E-mail address: mike.ashfold@bris.ac.uk (M.N.R. Ashfold).

[1] Permanent address: Department of Mechanical Engineering, Ehime University, Matsuyama 79077, Japan.

[2] Present address: Department of Chemistry, University of Cambridge, Lensfield Road, Cambridge CB2 1EW, UK.

0925-9635/01/$ - see front matter
PII: S0925-9635(00)00444-1

and C_2 and CN radicals both along the length of, and transverse to, the arc jet axis. Abel inversion methods [11] have been used to transform measured species selected, spatially resolved, OES intensities into radial distributions of the chosen emitting species. OES, of course, only gives access to excited state species which, given their low relative abundance, are generally considered not to be important in the overall diamond growth process. More detailed interpretation of such measurements and, particularly, their relation to the more abundant ground state species requires rather detailed knowledge of both the production and quenching mechanisms for these excited species, but the spatial variations and trends with changes in process condition can serve as a useful plasma diagnostic.

2. Experimental

2.1. Film deposition and characterization

Fig. 1 provides a schematic illustration of the experimental apparatus used for film deposition and for observing optical emission from the plasma. The DC-arc jet plasma is generated using a twin torch head arrangement (Aeroplasma Corp.) designed to operate at up to 10 kW discharge power. Twin torch arrangements such as this provide improved plasma stability over single torch systems. The N-torch is designed to propagate a stable plasma flow by incorporating a secondary spiral jet stream of pre-mixed Ar and H_2 into the primary Ar plasma prior to the converging-diverging nozzle orifice. Methane and, when required, N_2 are introduced into the Ar/H_2 plasma through an annular injection ring (I in Fig. 1) positioned 100 mm downstream from the nozzle. All gas flows are metered using appropriate mass flow controllers (MKS). The plasma impinges normal to the surface of a water-cooled polished (using 1 μm grade diamond dust) molybdenum substrate (16 mm diameter), positioned 155 mm from the nozzle exit, on which the polycrystalline diamond film condenses. The pressure in the reaction chamber is monitored continually and controlled at 50 torr. The chamber is water-cooled and evacuated to a base pressure of 50 mtorr using a two stage rotary pump (Edwards E2M40). All films produced for this study were grown at a substrate temperature of 880°C, measured by a two-colour optical pyrometer. Each deposition lasted one hour, with identical $CH_4/H_2/Ar$ flow rates, variable N_2 additions, and a constant input power of 5.9 kW (78 V, 76 A). The resulting films delaminate on cooling and are analysed as free-standing. Growth rate and surface topology are revealed by SEM, while laser Raman spectroscopy (Renishaw, He-Cd laser excitation at 325 nm) provides an indication of film quality.

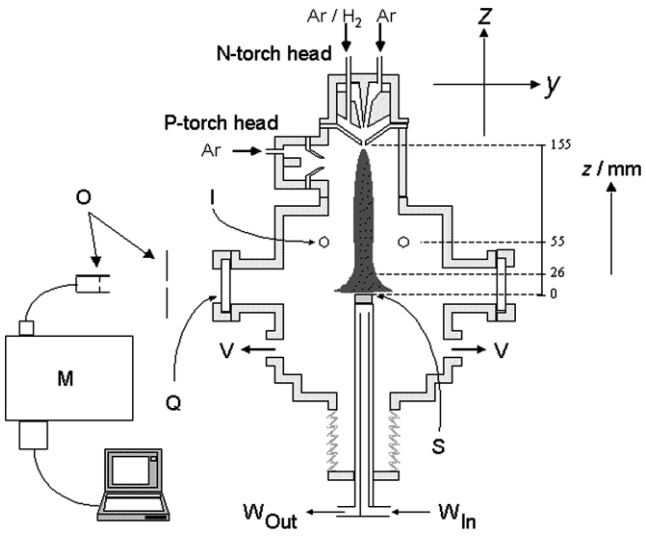

Fig. 1. Section (schematic) through the apparatus for film deposition and OES measurements. The plasma jet propagates in the $-z$ direction, with the surface of the substrate (S) positioned at $z = 0$. Optical emission (in the $-y$ direction) is viewed through a quartz window (Q), a train of iris diaphragms and a fibre optic bundle (O), dispersed with the monochromator (M) and detected with a CCD array. The x-axis is orthogonal to the plane of the figure. Key to other components: I, injection ring for CH_4 (and N_2); V, connections to rotary pump; W, cooling water (in and out).

2.2. Optical emission spectroscopy

Spatially resolved distributions of optical emission from electronically excited H atoms, and C_2 and CN radicals have been measured. A 2 mm-diameter column of the plume emission was defined by a combination of two irises positioned, in series, in front of a quartz fibre optic bundle all of which were mounted on a common two-dimensional translation stage. Optical emission was collected at 1-mm intervals along the z-axis in the region $0 < z < 26$ mm defined in Fig. 1, and at 2-mm intervals in the range $-4 < x < 16$ mm (i.e. out of plane depicted in Fig. 1) for several different fixed z values, each separated by 5 mm, in front of the substrate surface and perpendicular to the plasma flow. Spectra were collected using a UV extended CCD array detector mounted onto either a 12.5-cm monochromator (Oriel Instaspec IV, 600 lines mm^{-1} ruled grating) or a 0.5-m monochromator (Spex 1870, equipped with a 2400-lines mm^{-1} holographic grating) depending on the wavelength range and resolution required. The CCD array detector allows simultaneous collection of all emission within a chosen wavelength range.

3. Results and discussion

Diamond films deposited and OES measurements taken in this study all used a fixed $Ar/H_2/CH_4$ feed

gas ratio and flow rate (Ar 87.83%, H_2 11.59%, CH_4 0.58%, total flow rate 13.8 slm) with the addition of various known quantities of N_2 in the range 0–20 sccm (for film growth) and 0–100 sccm for OES studies.

3.1. Film deposition

A series of films were deposited with different N_2 flow rates each for 1-h growth duration. Cross-sectional SEM images allow investigation of the film morphology and estimation of the deposition rate, measured at the film centre, as a function of added N_2. Representative SEM images of films grown with N_2 additions of, respectively, 0 and 1 sccm are shown as insets in Fig. 2a. These illustrate that N_2 addition to the process gas mixture affects the film morphology. Diamond films grown with no added N_2 are predominantly (111) faceted, and exhibit twinning and secondary nucleation while, with addition of 1 sccm N_2, a central region of largely (100) growth is formed, in which some of the crystallites exhibit facets approaching ~ 60 μm in size. Further addition of N_2 promotes the growth of ballas-type features. Fig. 2a shows the measured growth rate (μm h^{-1}) increasing with trace N_2 additions but then decreasing with increasing N_2; since the films grown at higher N_2 partial pressures are increasingly graphitic, and thus have lower density, the growth rate defined as deposited mass per hour would fall off even more steeply with increasing N_2.

Laser Raman spectroscopy is also used to assess the quality of the as-grown films. Representative spectra of films grown with addition of, respectively, 0 and 10 sccm of N_2 to the process gas mixture are shown as insets in Fig. 2b, while the main body of this figure illustrates the reduction in film quality that accompanies increased N_2 flow rates. Quality here is represented by the quotient, Q_D, where

$$Q_D = I_D/(I_D + I_G) \quad (1)$$

and I_D and I_G are, respectively, the relative intensities of the sp^3 C peak (at a Stokes shift of ~ 1332 cm^{-1}) and the sp^2 C feature (centred at ~ 1550 cm^{-1}). Careful studies in other CVD environments have generally shown an improvement in diamond film quality upon small N_2 additions, followed by a decline at higher levels of added nitrogen, but we see only a reduction in Q_D with increasing N_2 additions — hinting at an obstructive role for nitrogen in the diamond step growth mechanism. This may reflect the poorer base vacuum of the large DC-arc plasma jet reactor, such that it is always operating at a background partial pressure of air and thus nitrogen above those for optimal diamond film quality. Consistent with this, we observe a weak Raman feature at ~ 2328 cm^{-1} which, it has been suggested [12], should be associated with a carbon-nitrogen stretching mode. This feature is present in all Raman spectra measured in this study, including those of films grown in a standard $CH_4/H_2/Ar$ gas mixture with no intentionally added N_2. Unfortunately, it is not sufficiently intense for reliable inter-film comparisons. Photoluminescence studies following excitation at longer wavelengths will be useful in assessing the extent of N incorporation in these films grown by DC-arc plasma jet CVD.

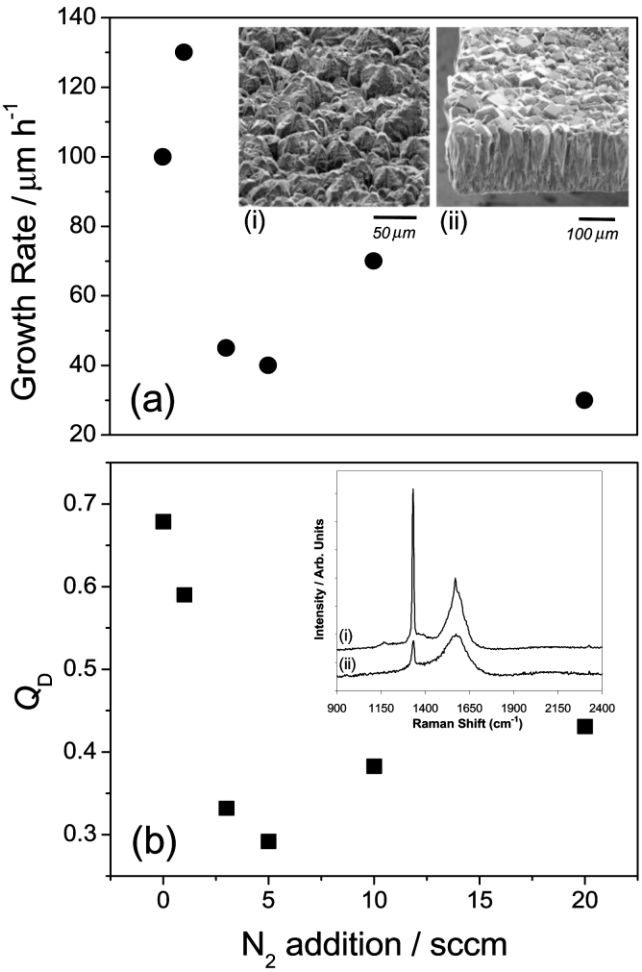

Fig. 2. Plots showing the influence of added N_2 on (a) film growth rate and (b) film quality, (Q_D). SEM images of the central portions of films deposited with: (i) 0; and (ii) 1 sccm added N_2 are shown as insets in (a). The inset in (b) displays laser Raman spectra of films grown with 0 and 10 sccm (upper and lower traces, respectively) of N_2 added to the standard $CH_4/H_2/Ar$ process gas mixture, scaled and offset vertically for clarity of presentation.

3.2. OES studies

The emission spectra of $CH_4/H_2/Ar/N_2$ plasmas are dominated by the $C_2(d^3\Pi_g \rightarrow a^3\Pi_u)$ Swan band system but, as Fig. 3a shows, emission from both atomic hydrogen (Balmer-α transition, henceforth H_α, at 656.3 nm) and the $CN(B^2\Sigma^+ \rightarrow X^2\Sigma^+)$ system at wavelengths ~ 388 nm are also visible. $CH(A^2\Delta \rightarrow X^2\Pi)$ emission at

wavelengths of ~431.4 nm is discernible, but so weak in comparison with the Swan band system that it is not considered in this study. All emission lines from Ar (neutral and ionic) observed from the pure Ar plasma are quenched on addition of H_2, thus preventing their use in actinometric measurements. Fig. 3b shows the measured variation of the CN(B → X) and C_2(d → a) emission intensities as a function of added N_2. The growth in CN(B → X) emission clearly implicates nitrogen as a species that participates in the gas-phase chemistry within the plasma plume, while the plot of C_2(d → a) emission intensities serves to illustrate the substantial quenching induced by the addition of just a trace of N_2. Consistent with the previous discussion regarding the inevitable presence of some background N_2 in the process gas mixture, very weak CN(B → X) emission is observed with (nominally) 0 sccm added N_2; extrapolating the data displayed in Fig. 3b provide an upper limit estimate of 2.2 sccm (~160 ppm) as the 'flow rate equivalent' N_2 content under these conditions.

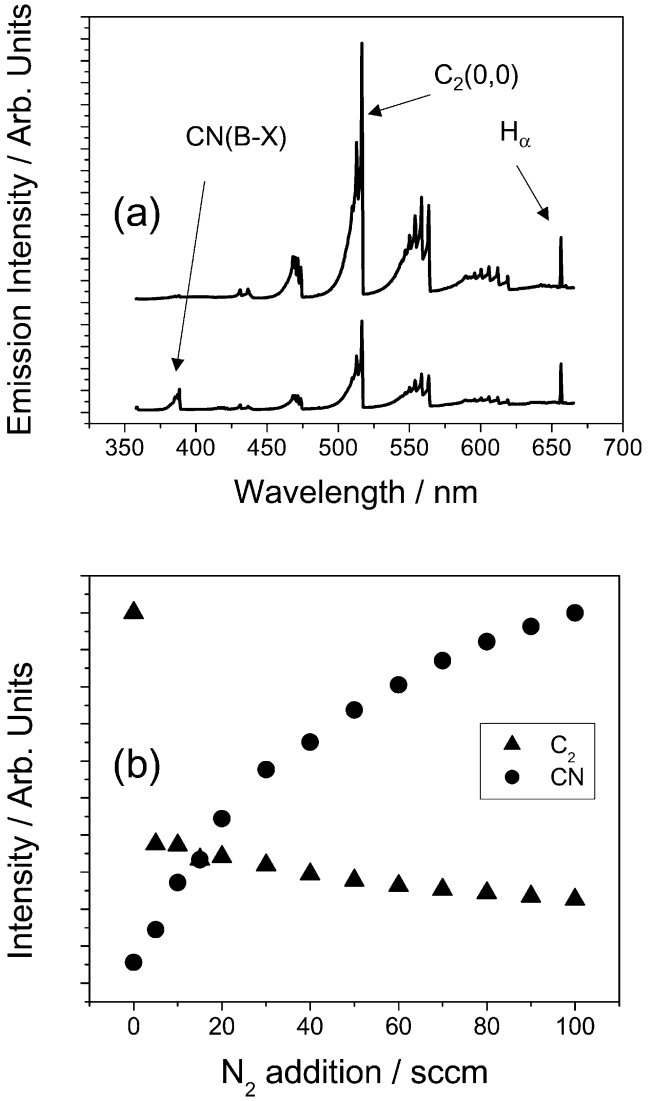

Fig. 3. (a) Wavelength dispersed optical emission spectra obtained viewing at $z = 10$ mm using the standard $CH_4/H_2/Ar$ process gas mixture with addition of 0 (upper trace) and 10 sccm of N_2 (lower trace), with the principle emission features indicated. The spectra, which were recorded with the same detector sensitivity and have been offset vertically for clarity of presentation, are not corrected for the wavelength dependent response of the monochromator grating and CCD array detector, which peaks at ~620 nm and is approximately three times less sensitive at the low end of the displayed wavelength range. (b) Increase in CN(B → X) emission intensity and concomitant quenching of C_2(d → a) emission that results from N_2 addition.

Measurements of the C_2(d → a) $\Delta v = 0$ progression recorded at higher resolution using the Spex monochromator show no obvious variation in band contour either with process conditions or with spatial location, though we note that this does not include the ~1 mm closest to the substrate surface (i.e. the region containing the boundary layer). This encourages the assumption that spatial variations in emission intensities monitored via the intense (0,0) band head at ~515 nm are representative of the entire distribution of emitting C_2 species. Fig. 4a,b shows plots of the spatially imaged C_2(d → a) and CN(B → X) emission intensities (at ~515 nm and ~388 nm, respectively, using a 2-mm diameter viewing column) as a function of position along z, measured from the substrate surface, while Fig. 4c shows a representative plot of C_2 emission intensity measured by translating the viewing column parallel to the substrate surface (i.e. along x) at a fixed z (6 mm from the substrate surface in this case).

Application of an Abel transform to this latter type of line-of-sight data set enables derivation of the radial dependence of emitting species within the plasma [11], if we assume that the plasma is optically thin at the emission wavelengths of interest. Such remains to be proved for the measurements reported here, particularly in the case of CN where the measured emissions terminate on the ground state, but the trends deduced in what follows remain valid even if the measurements are affected by preferential self-absorption at $x \sim 0$ mm. All measured species specific lateral emission intensity distributions, $I(x)$, appear symmetric at approximately $x = 0$ mm (as in Fig. 4c), thus satisfying the requirement of cylindrical symmetry for Abel inversion. Knowing $I(x)$ throughout the range $x = 0$ to $x = R$ (here chosen as 20 mm), Abel inversion yields the radial distribution of emitting species, $i(r)$, via the integral:

$$i(r) = \frac{1}{\pi}\int_{=r}^{+R} \frac{1}{(x^2 - r^2)^{1/2}} \frac{\mathrm{d}I(x)}{\mathrm{d}x}\mathrm{d}x \qquad (2)$$

The $i(r)$ profile so deduced for the case of C_2(d → a)

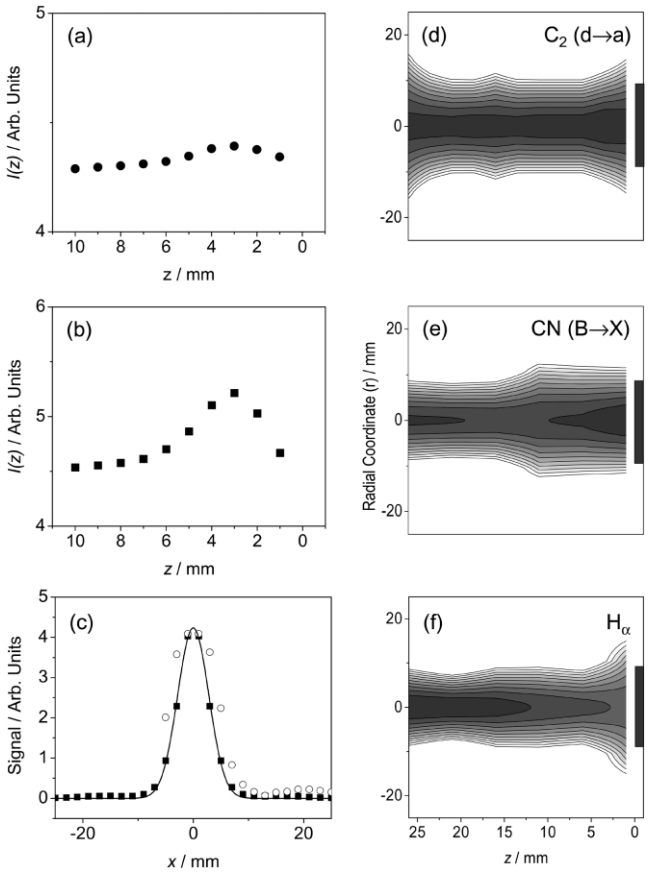

Fig. 4. (a) $C_2(d \rightarrow a)$ and (b) $CN(B \rightarrow X)$ emission intensities (at ~ 515 nm and ~ 388 nm, respectively, measured using a 2-mm diameter viewing column centred on $x = 0$) in the range $0 < z < 10$ mm. (c) $C_2(d \rightarrow a)$ emission intensity (○) measured by translating the viewing column across the range $-4 < x < 24$ mm, with $z = 6$ mm, together with the radial profile $i(r)$ derived using the Abel transform (■). Contour maps showing the deduced distribution of $C_2(d \rightarrow a)$, $CN(B \rightarrow X)$ and H_α emissions in (z, r) space are shown in (d–f), respectively, with the substrate face at $z = 0$ indicated in each case. Each distribution is displayed using a (logarithmic) 10-point grey scale, where dark indicates maximum emission intensity.

emission measured at $z = 6$ mm is also shown in Fig. 4c.

Given numerous such profiles, taken at many z values, for the $CN(B \rightarrow X)$, $C_2(d \rightarrow a)$ and H_α emissions, allows generation of spatially resolved emission intensity maps for each of these species. Fig. 4d–f shows such plots, as a function of z (horizontal axis, with the front face of the substrate at $z = 0$ indicated) and radial co-ordinate, r. All show some spatial inhomogeneity, with maximum emission intensities at the plume centre ($x \sim 0$). The CN and C_2 emission profiles show similar full width half maxima (FWHM) values in r, indicating efficient mixing within the plume, but the radial emission profile for H_α is narrower and more localized in the upstream, hotter, region of the plasma jet. Such trends have been reported previously, and discussed, following analysis of plume emissions from a lower power (2.3 kW) DC-arc plasma jet operating on an $Ar/H_2/CH_4$ gas mixture [13]. All are consistent with formation of C, N and H atoms by thermal decomposition of H_2, CH_4 and N_2 in the hottest regions of the plasma, and the increasing importance of subsequent recombination reactions to form species like C_2, CN, CH and H_2 further downstream, at cooler plasma temperatures. Where the plasma impinges on the substrate surface the large kinetic energy associated with the gas flow is converted into thermal energy, resulting in local gas heating. The $CN(B \rightarrow X)$ and $C_2(d \rightarrow a)$ emission intensity maps (Fig. 4d,e) both show local maxima near the surface which, as Yamaguchi et al. have commented [13], are probably more a reflection of this increase in local temperature than an indication of any increase in species number density. Finally, we note that the present work supports previous suggestions [13] that the observation of high C_2 emission intensities in a DC plasma jet correlates with higher quality diamond growth, in contrast to some of the earlier studies of microwave plasma enhanced CVD which found strong C_2 emission to be an indicator of degraded diamond film quality [14,15].

4. Conclusions

We report studies of diamond CVD at growth rates $> 100\ \mu m\ h^{-1}$ in a 10-kW DC-arc jet system, operating with $CH_4/H_2/Ar$ feedstock gas mixtures. Controlled addition of N_2 to the feedstock gas results in intense $CN(B \rightarrow X)$ emission and quenches $C_2(d \rightarrow a)$ and H_α emissions from the plasma. Abel transformation of species selective, spatially resolved OES measurements has allowed derivation of the longitudinal and lateral variation of emitting C_2, CN and H ($n = 3$) species within the plasma jet. SEM and laser Raman analyses indicate that such N_2 additions also lead to a reduction both in growth rate and quality of the resulting diamond film; the laser Raman measurements also provide evidence for nitrogen incorporation in the films.

Acknowledgements

We are grateful to De Beers Industrial Diamond Ltd. for the loan of the DC-arc plasma jet system, and to the EPSRC for equipment funding, a Senior Research Fellowship (M.N.R.A.) and a project studentship (J.A.S.). We are also grateful to Drs C.M. Western, E. Wrede and A.J. Orr-Ewing, and F. Claeyssens and G. Evans for their help with, and interest in, many aspects of this work.

References

[1] M.A. Cappelli, T.G. Owano, in: B. Dischler, C. Wild (Eds.), Low Pressure Synthetic Diamond, Springer, Berlin, 1998, pp. 59–84.
[2] M.E. Coltrin, D.S. Dandy, J. Appl. Phys. 74 (1993) 5803.
[3] S.L. Girshick, C. Li, B.W. Yu, H. Han, Plasma Chem. Plasma Proc. 13 (1993) 169.
[4] J. Luque, W. Juchmann, J.B. Jefferies, J. Appl. Phys. 82 (1997) 5.
[5] S. Jin, T.D. Moustakas, Appl. Phys. Lett. 65 (1994) 403.
[6] R.S. Tsang, C.A. Rego, P.W. May, M.N.R. Ashfold, K.N. Rosser, Diamond Relat. Mater. 6 (1997) 247.
[7] R. Locher, C. Wild, N. Herres, D. Behr, P. Koidl, Appl. Phys. Lett. 65 (1994) 34.
[8] P. Hartmann, R. Haubner, B. Lux, Diamond Relat. Mater. 6 (1997) 456.
[9] S.M. Leeds, P.W. May, M.N.R. Ashfold, K.N. Rosser, Diamond Relat. Mater. 8 (1999) 226.
[10] J.J. Schermer, F.K. de Theije, Diamond Relat. Mater. 8 (1999) 2127.
[11] A. Chelouah, E. Marode, G. Hartmann, J. Phys. D: Appl. Phys. 27 (1994) 770.
[12] H. Xin, C. Lin, W. Xu et al., J. Appl. Phys. 79 (1996) 2364.
[13] H. Yamaguchi, M. Ishii, K. Uematsu, S. Morimoto, Jpn. J. Appl. Phys. 35 (1996) 2306.
[14] W. Zhu, A. Inspektor, A.R. Badzian, T. McKenna, R. Messier, J. Appl. Phys. 68 (1990) 1489.
[15] Y. Muranaka, H. Yamashita, K. Sato, H. Miyadera, J. Appl. Phys. 67 (1990) 6247.